Nonlinear WEC modeling using Sparse Identification of Nonlinear Dynamics (SINDy)

Brittany Lydon, Brian Polagye, Michael Motley, and Steve Brunton

Abstract—**Modeling oscillating surge wave energy converter (OSWEC) systems is particularly challenging in realistic sea states where nonlinear WEC dynamics are common due to complex fluid-structure interaction, breaking waves, and other phenomena. Computationally efficient linear models can be inaccurate in energetic seas, while higher-fidelity numerical models are too computationally expensive for operational use, such as real-time state estimation and optimal control. To bridge this gap in modeling methods, we use Sparse Identification of Nonlinear Dynamics (SINDy) to build parsimonious nonlinear reduced-order models (ROMs) that describe OSWEC behavior in response to large-amplitude regular waves. Here, SINDy uses high-fidelity CFD data of nonlinear kinematic OSWEC behavior to identify ordinary differential equations (ODEs) that describe the time-evolution of measurement variables. We not only are able to develop reduced-order models that accurately describe both transient and steady-state system behavior, but we are able to gain valuable information on the underlying dynamics of the system. We find dominant cubic terms of the ROMs, indicative of higher-order nonlinearities in the system dynamics that can not be captured with purely linear techniques. These findings provide insight into modeling highly nonlinear WEC dynamics in response to energetic seas and present a framework for applying similar analysis to lab- or field-scale experiments.**

Index Terms—**wave energy, nonlinear dynamics, data-driven modeling, oscillating surge WEC**

I. Introduction

ONE of the most promising wave energy converter (WEC) technologies is the oscillating surge wave energy converter (OSWEC) [1] due to its ability to absorb power over a wide range of wave frequencies [2]. OSWECs, shown in the first panel of Fig. 1, are flap-type devices that primarily harness the surge motion of ocean waves, which causes a buoyant flap to oscillate in pitch about a bottom hinge [3]. These devices are particularly well suited for shallow ocean environments, which intensify the surge motion of wave orbitals and directional consistency due to shoaling [4]. They are also attractive for applications such as nearshore desalination, as the mechanical pitching motion can be directly translated to a pressure differential that drives a reverse osmosis process [5].

Although OSWECs operate in a single degree of freedom, the dynamics and resulting kinematics are difficult to describe in realistic sea states. This is partly because diffraction is one of the dominant forces that drives OSWEC dynamics, making common assumptions such as small-body approximations invalid for these systems [6]. The dynamics are also influenced by drag and viscous forces, resulting in complex nonlinear fluid-structure interaction that can not be fully described by linear potential flow theory, which can lead to errors in modeling and predicting energy absorption [7]. Because of these complexities, common linear design and modeling practices are often not suitable for OSWECs [2]. This motivated a significant body of work on developing high-fidelity models using computational fluid dynamics (CFD) [8]–[10] and smoothed particle hydrodynamics (SPH) [8], [11]–[16] to more accurately predict nonlinear OSWEC behavior. However, these models can take hours of clock time to simulate a single oscillation period of WEC behavior, making them unsuitable for real-time state estimation and optimal control schemes [17]. This motivates modeling techniques for OSWECs that are accurate enough to capture nonlinear OSWEC behavior in response to energetic seas, fast enough to be used in a real-time control scheme, such as model predictive control (MPC) [18], and can give insight on what is driving the nonlinear behavior in these systems.

One possible solution is using Sparse Identification of Nonlinear Dynamics (SINDy) [19] to build nonlinear reduced-order models (ROMs) that describe OSWEC behavior in response to large-amplitude regular waves. SINDy is an equation-free, data-driven algorithm that identifies dominant nonlinear functions present in system state dynamics using a library of nonlinear functions created from time series measurement data. The result is an ordinary differential equation (ODE) in time that can be solved from an initial condition to model and predict time behavior of the states. SINDy is parsimonious, meaning it uses a sparsity-promoting hyperparameter to find the the minimum number of model terms necessary to capture dominant dynamics. Because of this, ROMS discovered by SINDy are *in-*

The authors acknowledge support from the National Science Foundation AI Institute in Dynamic Systems (grant number 2112085), Department of Defense Naval Facilities Engineering Systems Command (contract N0002421D6400/N0002421F8712), and the National Science Foundation Graduate Research Fellowship (under Grant No. DGE-2140004).

B. Lydon is a graduate student at the University of Washington (e-mail: BrittLyd@uw.edu).

B. Polagye is a Professor at the University of Washington Department of Mechanical Engineering with affiliations with the Applied Physics Laboratory at UW and Pacific Northwest National Laboratory in Seattle, WA (e-mail: bpolagye@uw.edu).

M. Motley is an Associate Professor at the University of Washington Department of Civil and Environmental Engineering (e-mail: mrmotley@uw.edu).

S. Brunton is a Professor at the Univeristy of Washington Department of Mechanical Engineering and the Department of Applied Mathematics. He is the co-director of the AI Institute in Dynamical Systems at UW (e-mail: sbrunton@uw.edu).

Digital Object Identifier:
https://doi.org/10.36688/ewtec-2023-383

terpretable and *generalizable* that are not overfit to the data. Using the discovered ROMs and integrating in time, not only can SINDy provide time series models and future state predictions of OSWEC dynamics, it can also give insights into which variables are critical in describing the underlying nonlinear dynamics of the state. SINDy has been widely used in various scientific applications, including reduced-order modeling of fluid flows [20], [21], modeling complex aerodynamics off of structures [22] and oscillating foils [23], and modeling chemical reaction dynamics to identify the network's underlying mechanisms [24], but, to our knowledge, has not previously been used to model wave energy converters.

In this study, we use SINDy to describe the nonlinear dynamics of a lab-scale OSWEC in a wave tank subjected to large-amplitude regular waves. Our goal is to find a parsimonious ROM of OSWEC kinematics that accurately describes its nonlinear behavior and provides insight on the mechanisms leading to the nonlinear behavior. The remainder of the paper is laid out as follows: Section II describes the mathematical formulation of the SINDy algorithm, Section III describes the methods used for this study including data generation, processing, and evaluation, and Section IV describes the resulting ROM for angular acceleration and assesses how well SINDy can capture the nonlinear behavior observed in OSWEC dynamics.

II. Background

A. Sparse Identification of Nonlinear Dynamics (SINDy)

In this section, we outline a basic derivation of the SINDy algorithm and refer the reader to [19] for a full derivation and sample code. To begin, consider a generic set of equations that describes a dynamical system:

$$\frac{d}{dt}\boldsymbol{x}(t) = \boldsymbol{f}(\boldsymbol{x}, t), \tag{1}$$

where $\boldsymbol{x}(t) \in \mathbb{R}^n$ is a state vector of n state variables as a function of time t, and $\boldsymbol{f}$ is a (potentially nonlinear) function that represents the dynamics dictating the time behavior of the system. For many dynamical systems, the function $\boldsymbol{f}$ is *sparse* in the basis of potential functions that can be used to describe its dynamics [19]. The main idea of SINDy is to exploit this sparsity and determine the minimum terms in $\boldsymbol{f}$ to describe $\boldsymbol{x}$ using sparse regression. A visual schematic of the algorithm is shown in Fig. 1.

SINDy takes in snapshot data from each state variable, $\boldsymbol{x}_k$, and creates a data matrix, $\boldsymbol{X}$, whose columns represent each state. For this study, we are interested in modeling the kinematics of the OSWEC system, namely, angular acceleration as a function of velocity and position: $\ddot{\boldsymbol{\theta}} = \boldsymbol{f}(\boldsymbol{\theta}, \dot{\boldsymbol{\theta}})$, where $\ddot{\boldsymbol{\theta}}$ is the modelled variable and $\boldsymbol{\theta}$ and $\dot{\boldsymbol{\theta}}$ are the state variables. Because there are two state variables, the data matrix consists of two column vectors:

$$\boldsymbol{X} = \begin{bmatrix} | & | \\ \boldsymbol{\theta} & \dot{\boldsymbol{\theta}} \\ | & | \end{bmatrix} \in \mathbb{R}^{m \times 2}, \tag{2}$$

where each data vector contains m time steps. From this data matrix, SINDy generates a library of candidate functions, $\boldsymbol{\Lambda}(\boldsymbol{X})$:

$$\boldsymbol{\Lambda}(\boldsymbol{X}) = \begin{bmatrix} | & | & | & & | \\ 1 & \boldsymbol{X}^{P_1} & \boldsymbol{X}^{P_2} & \dots & \boldsymbol{X}^{P_N} \\ | & | & | & & | \end{bmatrix} \in \mathbb{R}^{m \times p}, \tag{3}$$

where $\boldsymbol{X}^{P_q}$ represents a polynomial factor of order q of data matrix $\boldsymbol{X}$ and N is the highest order polynomial considered. For example, for the data matrix described in Equation 2 with two states, $\boldsymbol{X}^{P_2} = [\boldsymbol{\theta}^2 \quad \boldsymbol{\theta}\dot{\boldsymbol{\theta}} \quad \dot{\boldsymbol{\theta}}^2]$. It is possible to include a wider range of candidate functions, such as trigonometric or hyperbolic functions, but because both the modelled and state variables are oscillatory, we expect the dynamics are likely to be well described using polynomial functions of the state variables, similar to other nonlinear oscillatory systems such as a Duffing or Van der Pol oscillator [25]. In other words, we do not include trigonometric functions of our state variables in the function library because the states are inherently periodic, so applying a trigonometric function to the states would be akin to taking a sine function of a sine wave.

Using the library of nonlinear functions, $\boldsymbol{\Lambda}(\boldsymbol{X})$, we can set up a regression problem to find a ROM for $\ddot{\boldsymbol{\theta}}$:

$$\ddot{\boldsymbol{\theta}} = \boldsymbol{\Lambda}(\boldsymbol{X})\boldsymbol{\xi}, \tag{4}$$

where we aim to find function weights $\boldsymbol{\xi} \in \mathbb{R}^{p \times 1}$ that result in the fewest number of active terms in $\boldsymbol{\Lambda}(\boldsymbol{X})$ to accurately describe, $\ddot{\boldsymbol{\theta}}$. The variable we are interested in modeling, in this case $\ddot{\boldsymbol{\theta}}$, can either be measured similarly to the state variables, or calculated numerically from the state variables. We use the least absolute shrinkage and selection operator (LASSO) [26], [27] to find $\boldsymbol{\xi}$:

$$\arg\min_{\boldsymbol{\xi}} \left|\left| \ddot{\boldsymbol{\theta}} - \boldsymbol{\Lambda}(\boldsymbol{X})\boldsymbol{\xi} \right|\right|_2 + \lambda \left|\left|\boldsymbol{\xi}\right|\right|_1, \tag{5}$$

where λ is a hyperparameter that enforces sparsity by penalizing the sum of the terms in $\boldsymbol{\xi}$. λ is tunable and can be chosen such that parsimony is achieved, i.e. the dynamics are accurately represented, but not overfit. Once $\boldsymbol{\xi}$ is known, we have a symbolic equation that describes the reduced order model (ROM) of $\ddot{\theta}(t)$:

$$\ddot{\theta}(t) = \boldsymbol{\Lambda}(\boldsymbol{x})\boldsymbol{\xi}, \tag{6}$$

where $\boldsymbol{\Lambda}(\boldsymbol{x})$ is a library of symbolic functions composed of symbolic variables $\theta(t)$ and $\dot{\theta}(t)$, not data. This form of output is advantageous for multiple reasons. First, angular acceleration can be calculated from instantaneous measurements of angular position and velocity. Second, the model can be applied to different time sections of interest with a similar level of accuracy as the section of data it was trained on. Third, based on the active functions in Equation 6, we can identify drivers of nonlinear behavior in dynamics, $\ddot{\theta}(t)$, by the nonzero terms in $\boldsymbol{\xi}$ and, from this, learn more about the underlying dynamics of the system. Finally, having a closed-form expression for the modelled variable can be critical for important WEC applications such as future-state prediction or optimal control, where a fast and accurate system model is needed.

TABLE I
RELEVANT VALUES FOR OPENFOAM SIMULATION SETUP.

Description	Symbol	Value
flap mass	m_f	10.77 kg
flap inertia	I	0.1750 kg $\cdot$ m^2
flap width	w	0.65 m
flap height	h	0.341 m
flap thickness	a	0.1 m
beach dimensions	b_1	4.82 m
	b_2	1.30 m
	b_3	2.40 m
	b_4	3.70 m
	b_5	6.20 m
	c_1	0.150 m
	c_2	0.356 m
hinge height	c_3	0.476 m
water depth	d	0.71 m
wave period	T	2.0625 s
wave height	H	0.05 m

III. METHODS

An overview of the methods we used for this study are outlined in Fig. 1. There are three major steps, each outlined in detail in the following subsections: generate data, perform SINDy, and evaluate model output.

A. Generate and process data

We begin by generating the data that will be input into the SINDy model (Block I in Fig. 1). We generate this data using an OpenFOAM v2012 model of a lab-scale OSWEC described in [28]. A schematic of the simulation is given in Fig. 2. The model is based on experiments run at Queen's University in Belfast [10]. The wave tank is 4.58 meters wide and 20 meters long with a progressive sloped bathymetry with two flat sections connected by linear ramps. There is a wavemaker that generates regular, linear waves with a period of 2.0625 seconds and a height of 0.05 meters. Although Fig. 2 shows the OSWEC composed of a base and flap, the OpenFOAM simulation only models the flap with a constraint that it oscillates at a hinge oriented with the cross-dimension of the tank and located 0.476 m from the bottom of the tank. The OSWEC flap is 0.65 meters wide and 0.34 meters tall. Relevant system parameters are summarized in Table III-A and we refer the reader to [28] for further simulation details on wave tank, OSWEC, and wave parameters.

OpenFOAM is a finite volume fluid solver that can be combined with a rigid body solver to model complex fluid-structure interaction. Because we aim to model nonlinear OSWEC behavior, we want the OSWEC to experience large rotations. However, this can complicate the meshing process in the numerical simulation, as large rotations can cause the mesh to degrade and become skewed [10], [29]. To overcome this, this OpenFOAM model uses an overset grid, where the simulation domain contained two meshes: a background mesh of the wave tank and a overset body-fitted mesh around the flap [30]. Using this overset grid method, neither mesh is deformed throughout the simulation. Instead, the overset mesh moves with the rigid flap and flow field values are interpolated from the boundary of the background and overset mesh. There have been several recent studies have utilized this meshing method to model numerical wave tanks [31] and WEC hydrodynamics [32]–[37]. Further details on meshing and simulation details are provided in [28].

Using the OpenFOAM simulation, we extract flap position, $\boldsymbol{\theta}$, and angular velocity, $\dot{\boldsymbol{\theta}}$, as inputs to the SINDy algorithm. The flap experiences large displacements of about $\pm 48°$. Time series of OSWEC kinematics from the OpenFOAM model are shown in Fig. 3. We cut the time series into a six second window (almost three oscillation periods) to use as training data for SINDy. We then arrange the data into the data matrix $\boldsymbol{X}$, which is used to generate the library of functions, $\boldsymbol{\Lambda}$, shown in the schematic in Fig. 1. For this case, data matrix $\boldsymbol{X}$ has two columns, the first column is the time series data for angular position, $\boldsymbol{\theta}$, and the second is the time series data for angular velocity, $\dot{\boldsymbol{\theta}}$. Next, we calculate $\ddot{\boldsymbol{\theta}}$ by applying a fourth-order numerical differentiation scheme to $\dot{\boldsymbol{\theta}}$. The calculated angular acceleration, $\ddot{\boldsymbol{\theta}}$ is shown in Fig. 3 and will serve as our modeled variable on the left hand side of Equation 4.

B. Run SINDy

Now that we have our data matrices, we can input them to the SINDy algorithm to get a ROM for angular acceleration, $\ddot{\boldsymbol{\theta}}$ (Block II in Fig. 1). In other words, we aim to find a function $\boldsymbol{f}$ such that:

$$\ddot{\boldsymbol{\theta}} = \boldsymbol{f}(\boldsymbol{\theta}, \dot{\boldsymbol{\theta}}). \tag{7}$$

We emphasize that this is non-trivial because, while $\ddot{\boldsymbol{\theta}}$ is given by differentiation of $\dot{\boldsymbol{\theta}}$, this function can estimate $\ddot{\boldsymbol{\theta}}$ from instantaneous observations. We run the SINDy algorithm over a range of the two user-defined parameters: maximum polynomial order, N, and the sparsity-promoting hyperparameter, λ. Although an iterative process, the cost of running the SINDy algorithm over a range of parameters is significantly less than that of high-fidelity modeling, making it still computationally efficient.

C. Evaluate ROM output

Finally, to assess how well the ROM describes the nonlinear dynamics (Block III in Fig. 1), we evaluate the error between the OpenFOAM output and the ROM produced by SINDy for $\ddot{\boldsymbol{\theta}}$. We calculate the error as:

$$\text{error} = ||\ddot{\boldsymbol{\theta}}_{SINDy} - \ddot{\boldsymbol{\theta}}||_2. \tag{8}$$

We look at the error value over the tested range of model parameters to determine what values result in a parsimonious, yet accurate, model (i.e., the best-fit for the nonlinear dynamics using the fewest active terms in $\boldsymbol{\Lambda}(\boldsymbol{X})$).

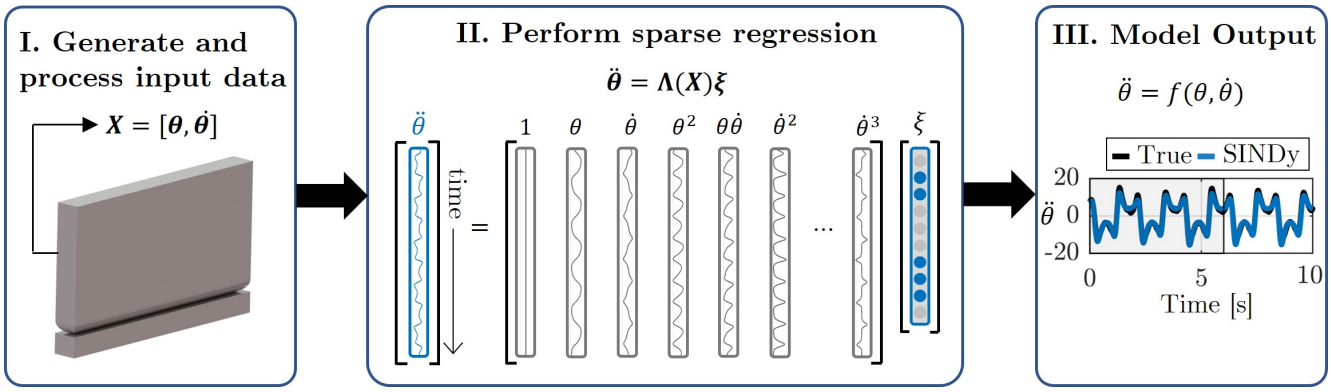

Fig. 1. SINDy data analysis workflow. We begin by generating nonlinear kinematic data from OpenFOAM (Block I). After preprocessing the data, we input it into the SINDy algorithm (Block II), which first creates a library of nonlinear functions of order N, $\mathbf{\Lambda}(\boldsymbol{X})$, from data $\boldsymbol{X}$. SINDy then uses a sparse regression algorithm to solve $\ddot{\boldsymbol{\theta}} = \mathbf{\Lambda}(\boldsymbol{X})\boldsymbol{\xi}$ for coefficients, $\boldsymbol{\xi}$. The sparsity-promoting parameter λ is tuned to ensure $\boldsymbol{\xi}$ has the minimum number of terms to accurately describe dynamics $\ddot{\boldsymbol{\theta}}$. After choosing N and λ, we compare the ROM to original data (Block III) to assess if the dominant dynamics were adequately captured.

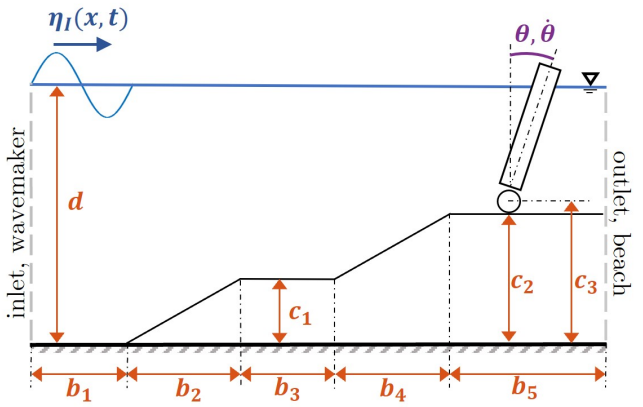

Fig. 2. Schematic of the OpenFOAM simulation setup [28], based on experiments in [10]. The incident wave input is shown in blue, with measured system states in green and dimensions in purple. The values of the dimensions are give in Table III-A.

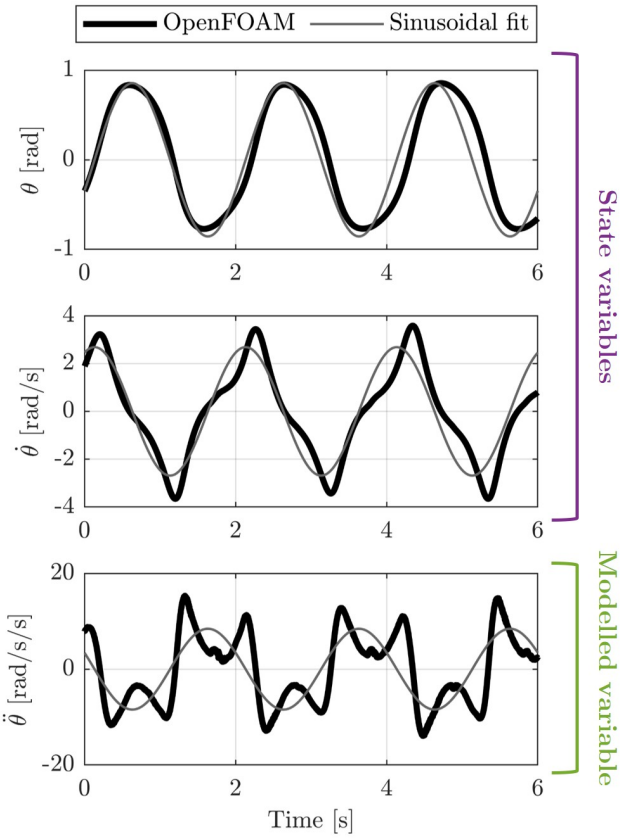

Fig. 3. Output from OpenFOAM (black) of angular position (top), $\boldsymbol{\theta}$, velocity (middle), $\dot{\boldsymbol{\theta}}$, and acceleration (bottom), $\ddot{\boldsymbol{\theta}}$. Gray curves represent purely linear, sinusoidal behavior with the same starting conditions and an oscillation period equal to the wave period, as is often the kinematic behavior of linear modeling techniques. The OpenFOAM output exhibits nonlinear behavior including time-varying oscillation frequency and evident cubic nonlinearity in $\dot{\boldsymbol{\theta}}$. $\boldsymbol{\theta}$ and $\dot{\boldsymbol{\theta}}$ are the state data we input to the SINDy algorithm to get an output for a ROM of $\ddot{\boldsymbol{\theta}} = \boldsymbol{f}(\boldsymbol{\theta}, \dot{\boldsymbol{\theta}})$.

D. Nonlinear kinematics

The upper two panels in Fig. 3 show the kinematic state variables used to train the model – angular position $\boldsymbol{\theta}$ and angular velocity $\dot{\boldsymbol{\theta}}$. These kinematics demonstrate complex, nonlinear behavior that can not be captured by linear potential flow models. Linear models often assume that the flap oscillates as a perfect sinusoid with an oscillation frequency equal to that of the incident wave, such that: $\theta_{\text{linear}}(t) = A\sin(\omega t + \phi)$, where $\omega = 2\pi/T$, and T is the incident wave period [38]–[40]. We compare the OpenFOAM output against this linear representation, with parameters A and ϕ determined from the state initial condition and maximum amplitude of the OpenFOAM model, respectively. Similarly, we calculate the derivatives of the linear representation to compare to $\dot{\boldsymbol{\theta}}$ and $\ddot{\boldsymbol{\theta}}$. Comparing these two curves highlights the nonlinearities present in the state variables. First, the OpenFOAM kinematics oscillate at a slightly different frequency than the incident wave. In addition, the shape of the oscillations for the kinematics vary from a simple sinusoid. The shape of $\boldsymbol{\theta}$ (a) closely resembles a sinusoid, with some asymmetry about the peak, but in taking the derivatives the nonlinearity is much more evident, and it is clear that higher order functions are required to describe the behavior than a simple sinusoid. For example, there is evident cubic behavior in the oscillations for angular velocity (b). And finally, the peaks in amplitude of the OpenFOAM angular velocity (b) and acceleration (c) exceed that of the linear approximation. It is important to model these peaks well to ensure

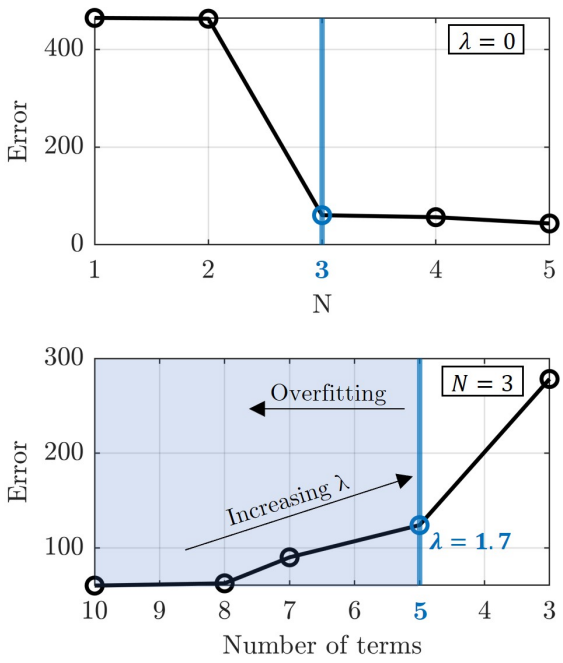

Fig. 4. (Top) Error as a function of maximum polynomial order, N, for $\lambda = 0$, i.e., including all terms, no sparsity enforced. Error drops significantly when considering cubic nonlinearity, with little accuracy gained when considering higher orders. This behavior also occurs for all other λ values. We choose $N = 3$ based on this drastic decrease in error. (Bottom) Error as a function of number of terms included in ROM for $N = 3$. Number of terms decrease as λ increases and we further enforce sparsity. Error increases drastically when the number of terms drops below five, therefore we choose $\lambda = 1.7$ to obtain a parsimonious model that is accurate but not overfit.

structural integrity and power conversion efficiency for the device.

IV. Results and Discussion

Fig. 4 summarizes the results of iterating the SINDy algorithm over a range of maximum polynomial ordesr, N, and sparsity-promoting hyperparameters, λ. To choose the maximum polynomial order, N, we look at error as a function of N for $\lambda = 0$ case (no sparsity enforced), shown in Fig. 4. Although we are only showing the case for $\lambda = 0$, there is a similar pattern for all λ values tested. There is a drastic drop in error for $N > 2$, which implies that the cubic terms are vital to describing system dynamics. Since error does not significantly decrease for $N > 3$, we choose $N = 3$ as indicative of the lowest polynomial order that gives an accurate representation of the dynamics. After choosing N, we choose hyperparameter λ by considering error as a function of number of terms in the reduced order model for $\ddot{\boldsymbol{\theta}}$ (Fig. 4). As λ increases, the number of terms decreases as sparsity is more heavily weighted in Equation 5. By choosing the number of terms to include, we are implicitly describing a λ parameter. Although error increases as number of terms decreases (as expected), until the number of terms decreases below five terms the error is relatively stable. This means that five terms are the minimum

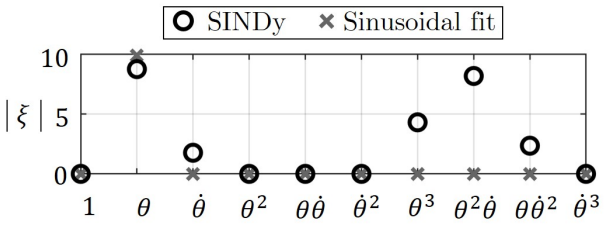

Fig. 5. Magnitude of function weights, $\boldsymbol{\xi}$, for SINDy model of angular acceleration, $\ddot{\boldsymbol{\theta}}$ with optimal conditions $N = 3$ and $\lambda = 1.7$ (black circles) and function weights of a purely sinusoidal, linear dynamics, $\ddot{\boldsymbol{\theta}} = -\omega^2\boldsymbol{\theta}$ (gray markers). Although both models have a large magnitude coefficient for $\boldsymbol{\theta}$, $\boldsymbol{\xi}$ has other nonzero coefficients for nonlinear terms, particularly cubic functions.

number of terms necessary to describe the dynamics, so we choose $\lambda = 1.7$ as our hyperparameter. Note that even though including more terms decreases the error in the ROM, including all of those terms means we are likely overfitting the data and failing to identify the most parsimonious model.

After choosing the maximum polynomial order, N, and sparsity-promoting hyperparameter, λ, we have an expression for angular acceleration with five remaining terms:

$$\ddot{\boldsymbol{\theta}} = -8.7\boldsymbol{\theta} + 1.8\dot{\boldsymbol{\theta}} + 4.3\boldsymbol{\theta}^3 - 8.2\boldsymbol{\theta}^2\dot{\boldsymbol{\theta}} - 2.4\boldsymbol{\theta}\dot{\boldsymbol{\theta}}^2. \quad (9)$$

To visualize the relative importance of each term in Equation 9, Fig. 5 shows the magnitude of function weights $\boldsymbol{\xi}$ for each candidate function in $\boldsymbol{\Lambda}(\boldsymbol{X})$. It is important to note that if this was a purely linear system and $\boldsymbol{\theta}$ could be represented by a sinusoid (such that $\ddot{\boldsymbol{\theta}} = -\omega^2\boldsymbol{\theta}$), the only nonzero component in ξ would be for the $\boldsymbol{\theta}$ function. Although the magnitude of the $\boldsymbol{\theta}$ function coefficient is the largest of $\boldsymbol{\xi}$, and of similar value of what it would be for the sinusoidal oscillation case, we see that there are several other active terms required for accurate modeling that deviate from the standard sinusoidal case. For example, both $\dot{\boldsymbol{\theta}}$ and $\boldsymbol{\theta}$ are needed to accurately describe $\ddot{\boldsymbol{\theta}}$, not just $\boldsymbol{\theta}$. Also, there are several higher order terms contributing to the dynamics of $\ddot{\boldsymbol{\theta}}$. In particular, the cubic terms contribute significantly to the ROM, including cross terms $\boldsymbol{\theta}^2\dot{\boldsymbol{\theta}}$ and $\boldsymbol{\theta}\dot{\boldsymbol{\theta}}^2$. In addition, all the quadratic terms are zeroed out, further emphasizing that there are dominant cubic nonlinearities represented in the dynamics that are necessary for accurate reconstruction. Note that even though only the odd orders of the library are activated, the active terms do not follow a traditional sine expansion of the state variables, which are already oscillatory in nature, due to the cross terms in Equation 9. This type of analysis is beneficial for multiple reasons. First, it informs the tools required for accurate modeling of OSWEC behavior in other systems. For example, if we were attempting to model a different OSWEC in response to a different incident wave, we would now know that for large rotations we will likely need to consider higher order terms up to the third order in our analysis. Without that knowledge, we would likely miss important dynamics that couldn't be captured with traditional linear methods. Second, the characteristics and order of the nonlinearity identified by SINDy

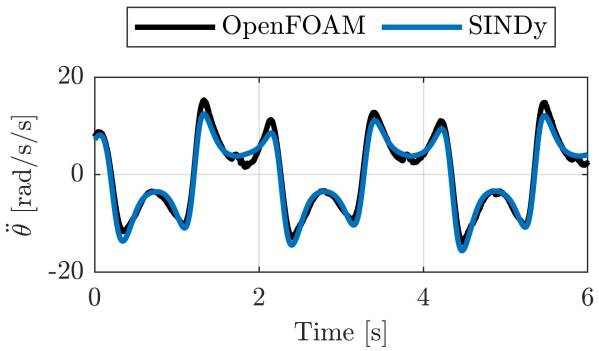

Fig. 6. OpenFOAM (black) and SINDy (blue) model of $\ddot{\boldsymbol{\theta}}$ in the training region.

can give important information on the nature of the system and how to control it. For example, it has been shown other oscillators with higher-order nonlinearities have a shift in eigenvalues of the system, which in term shift the oscillation frequency and amplitude, (both of which are evident in Fig. 3) [25]. This has important implications in resonant behavior as well as system control.

Fig. 6 compares the ROM output from SINDy for $\ddot{\boldsymbol{\theta}}$ to the output from OpenFOAM in the training region. The SINDy ROM describes the dynamics almost perfectly, which is what we expect since the model was trained on this data. There is slight underestimation on the positive peaks, but the nonlinear oscillation shape and frequency are well captured, unlike the case of sinusoidal motion (Fig. 3). This suggests that the ROM models the significant nonlinearities well in the training region. This is a promising result, but to confirm that Equation 9 describes the true dynamics of the full system, we need to look beyond the training region to see if the model can still accurately model data it was not trained on.

Fig. 7 compares the OpenFOAM and SINDy outputs for $\ddot{\boldsymbol{\theta}}$ over the full time series of OpenFOAM output. The time series includes three regions: the training region, a transient region before the training region where the wavemaker is ramping up, and a steady-state region after the training region. To be confident our model represents the true dynamics of the system, it is critical that it can accurately describe the system behavior in all three regions. Although we only trained the SINDy model on a small section of steady-state data, it is able to capture the dynamics well in all three regions. It is particularly promising that SINDy can describe the transient region because even though there are other reduced order modeling techniques that may be able to capture the higher order periodic behavior observed in the training region (such as a Fourier analysis or dynamic mode decomposition with time delays), this transient behavior would not be accurately represented unless it was included in the data. Although we may not be interested in this exact type of transient behavior, this shows that SINDy is able to capture transient kinematics, even when being trained on only steady-state data. Based on the accuracy with which the SINDy model describes the the full time series, we can be confident that this ROM is physically meaningful.

Now that we are confident that Equation 9 accurately describes the angular acceleration of the system, $\ddot{\boldsymbol{\theta}}$, we can integrate Equation 9 to evaluate the time evolution of state variables $\dot{\boldsymbol{\theta}}$ and $\boldsymbol{\theta}$. Fig. 8 shows the results of this integration from the same initial flap initial position and velocity conditions as OpenFOAM. There is an evident transient and steady-state region and the shape of the oscillations is similar between the OpenFOAM output and SINDy model, but there is a clear phase difference between the two. This can be a common result from integrating SINDy models, and we hypothesize that this is a consequence of a mismatch of excitations of the system. Since Equation 9 has no external excitation term, the nonzero initial conditions act as excitation to the system, while the OpenFOAM model is driven externally from the incident waves. Therefore, if the initial conditions of the OpenFOAM model do not excite the SINDy model in the same way as the external wave forcing, there will be a mismatch in phase as the transient region varies between the two models. We plan to investigate this further in future work. However, besides the evident phase shift, the two models both have a transient region, and steady state region, and oscillate with similar amplitude, structure, and frequency.

To more clearly visualize the differences in the integrated state variables from the SINDy model, Fig. 9 includes a 2.5 second phase shift that aligns the SINDy integration with the steady-state period. From this representation, it is clear that the SINDy model captures the steady-state region for both variables quite well, both in and outside of the training region. For the transient region, the SINDy model starts off modeling the behavior well, but then there is period of time in which the SINDy model does not match the OpenFOAM model. This could be due to a numerical artifact from the OpenFOAM model, or some underlying dynamics that are lost when integrating the SINDy model, even though angular acceleration is well-described throughout (Fig. 7).

Finally, Fig. 10 shows angular velocity $\dot{\boldsymbol{\theta}}$ as a function of angular position, $\boldsymbol{\theta}$ – a phase-space diagram of the state variables. Representing the variables this way allows us to compare the two models without comparing the two time series directly. Both models have a transient region that approaches a stable "limit cycle". The shape of the limit cycles for the OpenFOAM and SINDy models match well. The SINDy model also models the initial transient behavior well, but, as was evident in Fig. 9, there is discrepancy in the two models in the late transient region before the limit cycle. Again, this may be due to a numerical artifact or hidden dynamics not well described when integrated the Equation 9. Interestingly, we observe that the behavior of this system is similar to that of a Hopf bifurcation [41], with an unstable fixed point at the center of a stable limit cycle. Because this behavior has been well studied in other dynamical systems, existing work in modeling and controlling similar systems may

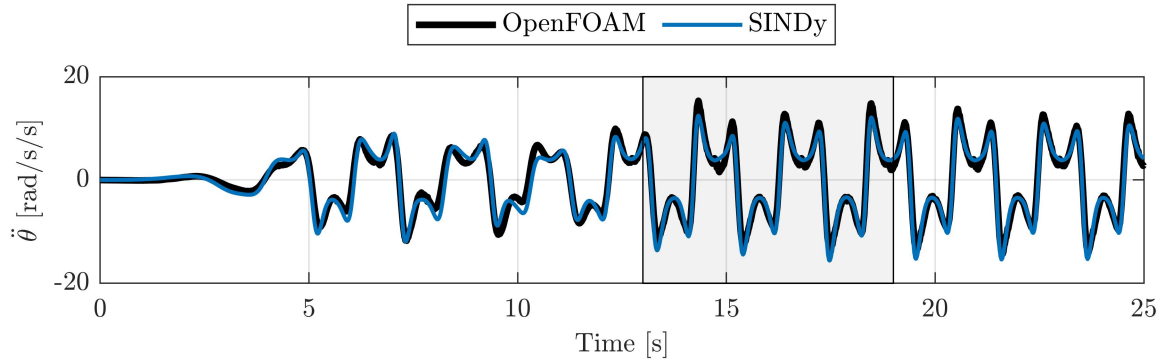

Fig. 7. OpenFOAM output (black) and SINDy output (blue) of angular acceleration, $\ddot{\boldsymbol{\theta}}$, in the training region (gray) and testing region (white). The SINDy model captures the dominating nonlinear features of the dynamics throughout both the training and testing region. In particular, the SINDy model is accurate even in the transient region before the training region, ensuring the model is describing the true system dynamics.

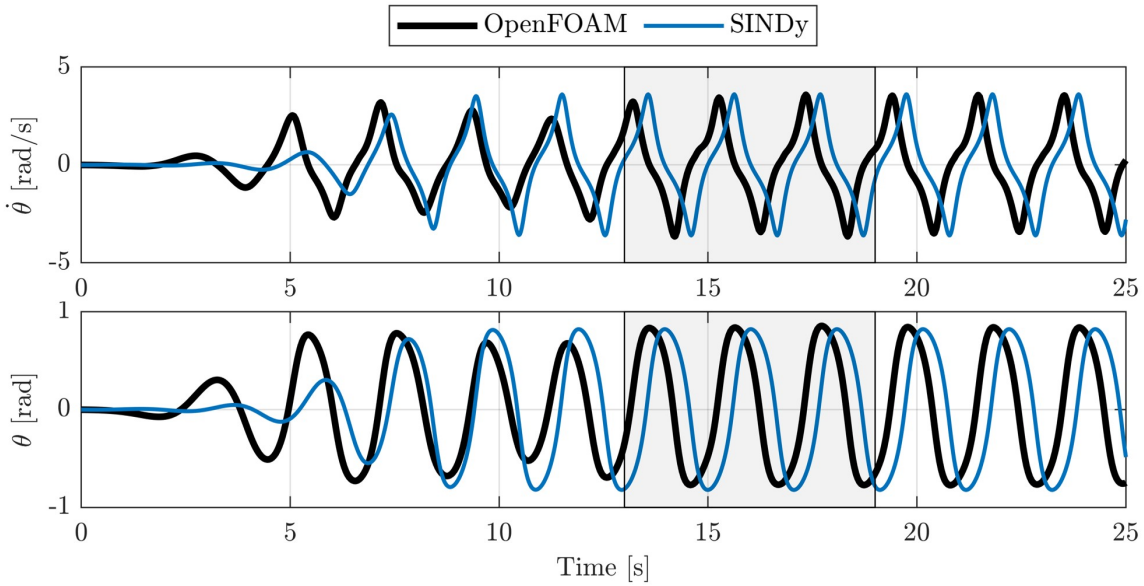

Fig. 8. OpenFOAM output (black) and integrated SINDy output (blue) of (top) angular velocity, $\dot{\boldsymbol{\theta}}$, and (bottom) angular position, $\boldsymbol{\theta}$. The training region is shown in gray. The SINDy model captures the dominating nonlinear features of the dynamics, but there is an evident phase shift between the two time series.

be able to inform further research in modeling and controlling similar WEC systems.

V. Conclusion

In this study, we use a nonlinear data-driven algorithm, SINDy, to generate accurate ROMs of nonlinear OSWEC kinematics using a limited number of terms. We used kinematic data from a high-fideltiy CFD simulation of an OSWEC in response to large amplitude regular waves, and showed the data to be highly nonlinear, with time-varying oscillation frequency and nonlinear oscillation profile. Using SINDy, we developed an accurate ROM for angular acceleration as a sum of nonlinear functions built from kinematic data (i.e., angular position and velocity). This ROM was not only able to model angular acceleration in the training data, but also accurately captured early transient behavior before the training region and steady-state behavior after. When we numerically integrate the ROM to obtain time series of angular velocity and position, there was a notable phase shift between the data and the integrated SINDy model, as well as amplitude and frequency deviations in part of the transient region. Agreement between input kinematics and integrated quantities is, however, excellent in the training and steady-state region.

By adjusting the maximum polynomial order in the model as well as the sparsity-promoting hyperparameter, we were able to ensure we had a parsimonious model that we could interpret to gain insight into the underlying nonlinear behavior. We found that to accurately describe the nonlinearity in the angular acceleration we must include cubic terms, and quadratic terms did not contribute to the dynamics, suggesting that future models need to consider terms up to the third order to be able to describe the dynamics well. Using this model, we can efficiently and accurately model and predict nonlinear OSWEC kinematics using only existing data.

In future work, we plan to build on this preliminary work in four main ways:

- **Expand variable type.** Although we used only

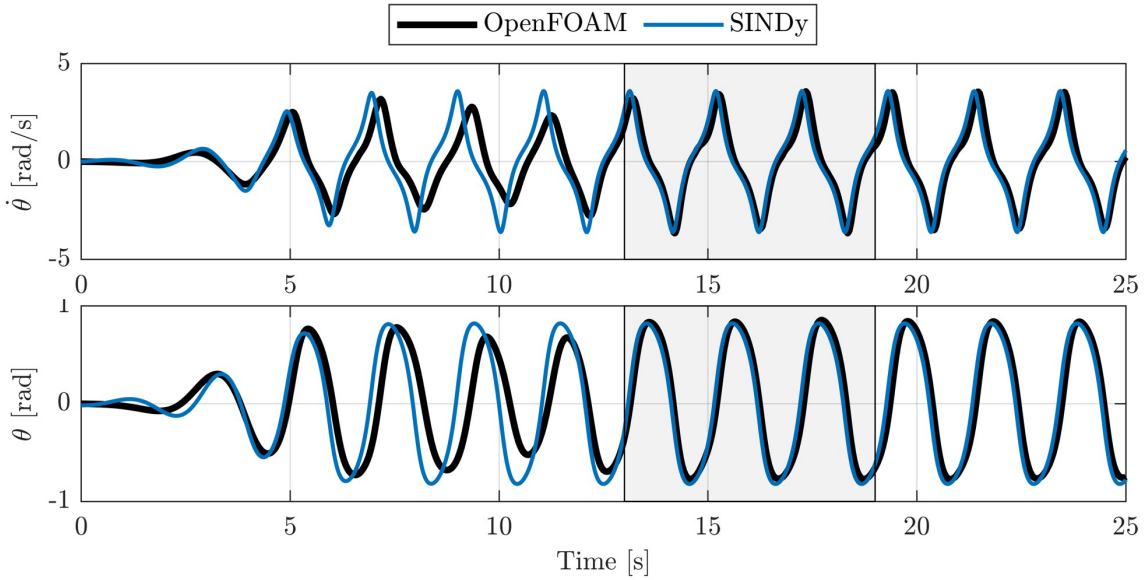

Fig. 9. OpenFOAM output (black) and integrated SINDy output (blue) of (top) angular velocity, $\dot{\boldsymbol{\theta}}$, and (bottom) angular position, $\boldsymbol{\theta}$. The SINDy time series is time-shifted to better match the phase of the OpenFOAM data. The training region is shown in gray. The two models are almost identical in the steady-state region, but there is some discrepancy in the transient region before the training data.

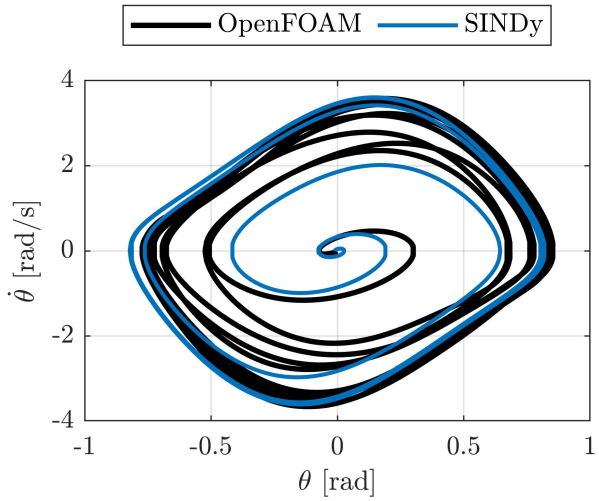

Fig. 10. Phase-space diagram of the two state variables: angular velocity, $\dot{\boldsymbol{\theta}}$, and angular position, $\boldsymbol{\theta}$, for both OpenFOAM (black) and SINDy model (blue). Both models have a transient region that leads to a "limit cycle". The SINDy model captures the initial transient behavior and the final limit cycle well, but there is discrepancy in the region between the initial transient and the limit cycle that is also evident in the time domain representations in Fig. 9.

kinematic OSWEC data in this study, this process is extendable to other dynamics, such as hydrodynamic force acting on the flap and torque about the bottom hinge. In addition to expanding the chosen modelled variables (the left-hand-side of Equation 4), we will expand the state variables included in the nonlinear function library to have a wider range of potential functions. We plan to include states such as hydrodynamic torque, pressure on the flap face, etc. This will provide more insight in the underlying system, as well as model more relevant variables for control.

- **Expand to experimental data.** Despite the generally high-fidelity nature of OpenFOAM, there will inevitably be aspects of experimental data not accurately captured in a numerical model, such as boundary effects and sensor noise. Therefore, we plan to extend this work to use experimental data as a SINDy input. This will help to evaluate the suitability of SINDy for more realistic WECs.
- **Compare to canonical systems.** There is an extensive body of work modeling and controlling nonlinear oscillatory dynamical systems [25]. Given the observed similarities to a Hopf bifurcation, we plan to compare the ROMs of this system to canonical nonlinear dynamical systems to further inform dynamics and control. We aim to draw these connections and leverage prior work in controlling similar nonlinear dynamical systems.
- **Apply to model predictive control.** Lastly, we want to apply this work to WEC control. ROMs from SINDy can be directly used to model predictive control schemes [18] and we aim to optimize power generation of OSWECs operating in highly energetic seas, where nonlinear behavior is expected.

Overall, SINDy appears to be a promising tool to generate reduced-order models of nonlinear WEC behavior and can provide insights into the underlying dynamics of these complex systems.

Acknowledgement

We thank Madeline Riddle for developing the OpenFOAM model that generated the data for this work. We also acknowledge support from the National Science Foundation AI Institute in Dynamic Systems (grant number 2112085), Department of Defense Naval Facilities Engineering Systems Command (contract N0002421D6400/N0002421F8712), and the National Science Foundation Graduate Research Fellowship (grant number DGE-2140004).

REFERENCES

[1] M. Folley, T. Whittaker, and M. Osterried, "The oscillating wave surge converter," in *The fourteenth international offshore and polar engineering conference*. OnePetro, 2004.

[2] M. Folley, A. Henry, and T. Whittaker, "Contrasting the hydrodynamics of heaving and surging wave energy converters," in *Proceedings of the 11th European Wave and Tidal Energy Conference, Nantes, France*, 2015, pp. 6–11.

[3] T. Whittaker, D. Collier, M. Folley, M. Osterried, A. Henry, and M. Crowley, "The development of oyster—a shallow water surging wave energy converter," in *Proceedings of the 7th European wave and tidal energy conference*, 2007, pp. 11–14.

[4] J. Falnes and A. Kurniawan, *Ocean waves and oscillating systems: linear interactions including wave-energy extraction*. Cambridge university press, 2020, vol. 8.

[5] M. Folley and T. Whittaker, "The cost of water from an autonomous wave-powered desalination plant," *Renewable Energy*, vol. 34, no. 1, pp. 75–81, 2009.

[6] G. Giorgi, M. Penalba, and J. Ringwood, "Nonlinear hydrodynamic force relevance for heaving point absorbers and oscillating surge converters," 2016.

[7] A. Babarit, J. Hals, M. J. Muliawan, A. Kurniawan, T. Moan, and J. Krokstad, "Numerical benchmarking study of a selection of wave energy converters," *Renewable energy*, vol. 41, pp. 44–63, 2012.

[8] Y. Wei and F. Dias, "Numerical study of three dimensional effects of wave impact on an oscillating wave surge converter," in *ASME 2015 34th International Conference on Ocean, Offshore and Arctic Engineering*. American Society of Mechanical Engineers Digital Collection, 2015.

[9] Y. Wei, T. Abadie, A. Henry, and F. Dias, "Wave interaction with an oscillating wave surge converter. part ii: Slamming," *Ocean Engineering*, vol. 113, pp. 319–334, 2016.

[10] P. Schmitt and B. Elsaesser, "On the use of openfoam to model oscillating wave surge converters," *Ocean Engineering*, vol. 108, pp. 98–104, 2015.

[11] Y. Wei, A. Rafiee, B. Elsaesser, and F. Dias, "Numerical simulation of an oscillating wave surge converter," in *ASME 2013 32nd International Conference on Ocean, Offshore and Arctic Engineering*. American Society of Mechanical Engineers Digital Collection, 2013.

[12] D.-W. Chen, S.-Y. Tzang, C.-M. Hsieh, Y.-C. Chow, J.-H. Chen, C.-C. Lin, and R. R.-J. Hwang, "Numerical modeling of wave-induced rotations of a bottom-hinged flapper with a sph model," *Journal of Marine Science and Technology*, vol. 22, no. 3, pp. 372–380, 2014.

[13] S. Yeylaghi, B. Moa, P. Oshkai, B. Buckham, and C. Crawford, "Isph modelling of an oscillating wave surge converter using an openmp-based parallel approach," *Journal of Ocean Engineering and Marine Energy*, vol. 2, no. 3, pp. 301–312, 2016.

[14] D. Zhang, Y. Shi, C. Huang, Y. Si, B. Huang, and W. Li, "Sph method with applications of oscillating wave surge converter," *Ocean Engineering*, vol. 152, pp. 273–285, 2018.

[15] Z. Wei, B. L. Edge, R. A. Dalrymple, and A. Hérault, "Modeling of wave energy converters by gpusph and project chrono," *Ocean Engineering*, vol. 183, pp. 332–349, 2019.

[16] M. Brito, R. Canelas, O. García-Feal, J. Domínguez, A. Crespo, R. Ferreira, M. Neves, and L. Teixeira, "A numerical tool for modelling oscillating wave surge converter with nonlinear mechanical constraints," *Renewable Energy*, vol. 146, pp. 2024–2043, 2020.

[17] S. L. Brunton and J. N. Kutz, *Data-driven science and engineering: Machine learning, dynamical systems, and control*. Cambridge University Press, 2022.

[18] E. Kaiser, J. N. Kutz, and S. L. Brunton, "Sparse identification of nonlinear dynamics for model predictive control in the low-data limit," *Proceedings of the Royal Society of London A*, vol. 474, no. 2219, 2018.

[19] S. L. Brunton, J. L. Proctor, and J. N. Kutz, "Discovering governing equations from data by sparse identification of nonlinear dynamical systems," *Proceedings of the national academy of sciences*, vol. 113, no. 15, pp. 3932–3937, 2016.

[20] K. Fukami, T. Murata, K. Zhang, and K. Fukagata, "Sparse identification of nonlinear dynamics with low-dimensionalized flow representations," *Journal of Fluid Mechanics*, vol. 926, p. A10, 2021.

[21] J.-C. Loiseau and S. L. Brunton, "Constrained sparse galerkin regression," *Journal of Fluid Mechanics*, vol. 838, pp. 42–67, 2018.

[22] S. Li, E. Kaiser, S. Laima, H. Li, S. L. Brunton, and J. N. Kutz, "Discovering time-varying aerodynamics of a prototype bridge by sparse identification of nonlinear dynamical systems," *Physical Review E*, vol. 100, no. 2, p. 022220, 2019.

[23] C. Sun, T. Tian, X. Zhu, and Z. Du, "Sparse identification of nonlinear unsteady aerodynamics of the oscillating airfoil," *Proceedings of the Institution of Mechanical Engineers, Part G: Journal of Aerospace Engineering*, vol. 235, no. 7, pp. 809–824, 2021.

[24] M. Hoffmann, C. Fröhner, and F. Noé, "Reactive sindy: Discovering governing reactions from concentration data," *The Journal of chemical physics*, vol. 150, no. 2, p. 025101, 2019.

[25] P. B. Kahn and Y. Zarmi, *Nonlinear dynamics: exploration through normal forms*. Courier Corporation, 2014.

[26] R. Tibshirani, "Regression shrinkage and selection via the lasso," *Journal of the Royal Statistical Society: Series B (Methodological)*, vol. 58, no. 1, pp. 267–288, 1996.

[27] T. Hastie, R. Tibshirani, J. H. Friedman, and J. H. Friedman, *The elements of statistical learning: data mining, inference, and prediction*. Springer, 2009, vol. 2.

[28] M. Riddle, "Cfd modeling of an oscillating wave surge converter using the overset grid method," Master's thesis, University of Washington, 2022.

[29] A. O. Winter and M. R. Motley, "Development of a fluid-structure interaction model of an oscillating wave surge converter using openfoam," in *International Conference on Offshore Mechanics and Arctic Engineering*, vol. 84416. American Society of Mechanical Engineers, 2020, p. V009T09A034.

[30] O. Ltd. (2019) Openfoam: User guide v2112. [Online]. Available: https://www.openfoam.com/documentation/guides/latest/doc/guide-overset.html

[31] H. Chen, L. Qian, Z. Ma, W. Bai, Y. Li, D. Causon, and C. Mingham, "Application of an overset mesh based numerical wave tank for modelling realistic free-surface hydrodynamic problems," *Ocean Engineering*, vol. 176, pp. 97–117, 2019.

[32] Z. Lin, H. Chen, L. Qian, Z. Ma, D. Causon, and C. Mingham, "Simulating focused wave impacts on point absorber wave energy converters," *Proceedings of the Institution of Civil Engineers-Engineering and Computational Mechanics*, vol. 174, no. 1, pp. 19–31, 2021.

[33] E. Katsidoniotaki and M. Göteman, "Comparison of dynamic mesh methods in openfoam for a wec in extreme waves," in *Developments in Renewable Energies Offshore*. CRC Press, 2020, pp. 214–222.

[34] C. Windt, J. Davidson, B. Akram, and J. V. Ringwood, "Performance assessment of the overset grid method for numerical wave tank experiments in the openfoam environment," in *International Conference on Offshore Mechanics and Arctic Engineering*, vol. 51319. American Society of Mechanical Engineers, 2018, p. V010T09A006.

[35] C. Windt, J. Davidson, D. D. Chandar, N. Faedo, and J. V. Ringwood, "Evaluation of the overset grid method for control studies of wave energy converters in openfoam numerical wave tanks," *Journal of Ocean Engineering and Marine Energy*, vol. 6, no. 1, pp. 55–70, 2020.

[36] D. P. Coiro, G. Troise, G. Calise, and N. Bizzarrini, "Wave energy conversion through a point pivoted absorber: Numerical and experimental tests on a scaled model," *Renewable Energy*, vol. 87, pp. 317–325, 2016.

[37] J. van Rij, Y.-H. Yu, Y. Guo, and R. G. Coe, "A wave energy converter design load case study," *Journal of Marine Science and Engineering*, vol. 7, no. 8, p. 250, 2019.

[38] E. Renzi and F. Dias, "Hydrodynamics of the oscillating wave surge converter in the open ocean," *European Journal of Mechanics-B/Fluids*, vol. 41, pp. 1–10, 2013.

[39] ——, "Resonant behaviour of an oscillating wave energy converter in a channel," *Journal of Fluid Mechanics*, vol. 701, pp. 482–510, 2012.

[40] J. Falnes, "Ocean waves and oscillating systems," *Ocean Waves and Oscillating Systems*, p. 285, 2005.

[41] J. E. Marsden and M. McCracken, *The Hopf bifurcation and its applications*. Springer Science & Business Media, 2012, vol. 19.